International Journal of Coal Geology 88 (2011) 31–40

Contents lists available at ScienceDirect

International Journal of Coal Geology

journal homepage: www.elsevier.com/locate/ijcoalgeo

Impact of transition from local swelling to macro swelling on the evolution of coal permeability

Jishan Liu [a,b,*], Jianguo Wang [a], Zhongwei Chen [a], Shugang Wang [c], Derek Elsworth [c], Yaodong Jiang [b]

[a] School of Mechanical and Chemical Engineering, The University of Western Australia, WA 6009, Australia
[b] State Key Laboratory for Coal Resources and Safe Mining, China University of Mining and Technology, Beijing,100083, China
[c] G³ Center, EMS Energy Institute, and Energy and Mineral Engineering, Pennsylvania State University, University Park, Pennsylvania, USA

ARTICLE INFO

Article history:
Received 13 May 2011
Received in revised form 28 July 2011
Accepted 28 July 2011
Available online 4 August 2011

Keywords:
Coal permeability
Coal swelling
Local swelling
Macro swelling

ABSTRACT

Laboratory observations have shown that coal permeability under the influence of gas adsorption can change instantaneously from reduction to enhancement. It is commonly believed that this instantaneous switching of permeability is due to the fact that the matrix swelling ultimately ceases at higher pressures and the influence of effective stresses take over. In this study, our previously-developed poroelastic model is used to uncover the true reason why coal permeability switches from reduction to enhancement. This goal is achieved through explicit simulations of the dynamic interactions between coal matrix swelling/shrinking and fracture aperture alteration, and translations of these interactions to perrmeability evolution under unconstrained swellings. Our results of this study have revealed the transition of coal matrix swelling from local swelling to macro-swelling as a novel mechanism for this switching. Our specific findings include: (1) at the initial stage of CO_2 injection, matrix swelling is localized within the vicinity of the fracture compartment. As the injection continues, the swelling zone is extending further into the matrix and becomes macro-swelling. Matrix properties control the swelling transition from local swelling to macro swelling; (2) matrix swelling processes control the evolution of coal permeability. When the swelling is localized, coal permeability is controlled by the internal fracture boundary condition and behaves volumetrically; when the swelling becomes macro-swelling, coal permeability is controlled by the external boundary condition and behaves non-volumetrically; and (3) matrix properties control the switch from local swelling to macro swelling and the associated switch in permeability behavior from reduction to recovery. Based on these findings, a permeability switching model has been proposed to represent the evolution of coal permeability under variable stress conditions. This model is verified against our experimental data. It is found that the model predictions are consistent with typical laboratory and in-situ observations available in lietratures.

1. Introduction

Gas transport in coal seams is significantly different from that in other types of rocks because of the phenomena of gas adsorption/desorption and coal swelling/shrinkage. The relative roles of stress level, gas pressure, gas composition, fracture geometry of coal, and water content are intimately connected to the processes of gas adsorption/desorption, diffusion, transport, and coal swelling/ shrinkage. As a direct consequence of these complex coal–gas interactions, coal permeability changes in both space and time.

Significant experimental efforts have been made to investigate gas permeability and its evolution in coal. Laboratory measured coal permeabilities to adsorbing gasses such as CH_4 and CO_2 are lower than those permeabilities to non-adsorbing or lightly adsorbing gasses such as argon and nitrogen (N_2) (Chen et al., 2011; Siriwardane et al., 2009; Somerton et al., 1975). The permeabilities may decrease by as much as five orders of magnitude if confining pressures vary from 0.1 to 70 *MPa* (Durucan and Edwards, 1986; Somerton et al., 1975). Under constant total stress, adsorbing gas permeability decreases with the increase of pore pressure due to coal swelling (Mazumder and Wolf, 2008; Pan et al., 2010; Robertson, 2005; Wang et al., 2010, 2011), and increases with the decrease of pore pressure due to matrix shrinkage (Cui and Bustin, 2005; Harpalani and Chen, 1997; Harpalani and Schraufnagel, 1990; Seidle and Huitt, 1995). Rebound pressure, which corresponds to the minimum permeability, was observed for CO_2 injection at 1.7 *MPa* (Pini et al., 2009), and at 7 *MPa* (Palmer and Mansoori, 1996; Shi and Durucan, 2004a, 2004b), recpectively. Permeability of adsorbing gas in coal is found to be a function of gas exposure time (Siriwardane et al., 2009). The pemeability is also influenced by water saturation (Han et al., 2010).

Based on field and laboratory experimental results, various coal permeability models have been proposed based on the fundamental principles of poroelasticity. These models could have different forms

* Corresponding author at: School of Mechanical and Chemical Engineering, The University of Western Australia, WA 6009, Australia.
E-mail address: jishan@cyllene.uwa.edu.au (J. Liu).

0166-5162/$ – see front matter © 2011 Elsevier B.V. All rights reserved.
doi:10.1016/j.coal.2011.07.008

after imposing specific conditions. When total stress has no change, both coal porosity and permeability are independent of the total stress. Under this condition, they can be expressed as a function of gas pressure and temperature only. If coal sample is in uniaxial strain and under no-changing overburden load, they can also be expressed as a function of gas pressure and temperature only. When the impact of coal fractures and gas compositions is considered, coal porosity and permeability models can be linked to fracture parameters and gas concentrations.

Permeability models were proposed for some idealized coal structures as well as specific boundary conditions. For example, Reiss (1980) developed the equations for permeability and porosity based on a collection of matchsticks and the collections of slabs and cubes. Gray (1987) considered that the changes in the cleat permeability were primarily controlled by the prevailing effective horizontal stresses that act across the cleats. Under the assumption of uniaxial strain, the influence of matrix shrinkage on the change of coal permeability was first incorporated into a permeability model. Gilman and Beckie (2000) assumed that an individual fracture reacts as an elastic body upon a change in the normal stress component and proposed a simplified mathematical model of methane movement in a coal seam. Their model takes into account the following features: a relatively regular cleat system, adsorptive methane storage, an extremely slow release mechanism of methane from the coal matrix into cleats, and a significant change of permeability due to desorption. Seidle and Huitt (1995) calculated the permeability increase due to matrix shrinkage alone by using a linear relationship between matrix shrinkage and pore pressure. Their model ignored the impact of coal compressibility and thus was limited to specific conditions in which sorption-induced strain (matrix swelling or shrinkage) dwarfs pressure-induced, elastic changes in cleat permeability (Robertson and Christiansen, 2008). Based on the matchstick geometry model and the relationship between permeability and porosity proposed by Seidle and Huitt (1995), Shi and Durucan (2004a, 2004b) presented a pore pressure-dependent cleat permeability model for gas-desorbing, linear elastic coalbeds under uniaxial strain conditions. In this model, the changes in the cleat permeability of coalbeds were assumed to be controlled by the prevailing effective horizontal stresses normal to the cleats. A widely used theoretical permeability model was derived by Palmer and Mansoori (1996) (called P&M model later). Their permeability in coals is as a function of effective stress and matrix shrinkage. The P&M model was improved and summarized by Palmer et al. (2007). Similarly, Pekot and Reeves (2002) have developed another permeability model which does not have a geomechanics framework, but instead extracts matrix strain changes from a Langmuir curve of strain versus reservoir pressure. It was assumed that strain was proportional to the gas concentration curve and matrix shrinkage was proportional to the adsorbed gas concentration change multiplied by shrinkage compressibility. This model has been compared to the P&M model, and concluded that the two models are essentially equivalent in saturated coals where the strain versus pressure function is proportional to the Langmuir isotherm (Palmer et al., 2007). Following the above work, Cui and Bustin (2005) quantitatively investigated the effects of reservoir pressure and sorption-induced volumetric strain on coal-seam permeability with constraints from the adsorption isotherm and associated volumetric strain and derived a stress-dependent permeability model. Focusing on the full separation of strain between matrix and cleat/fracture, Gu and Chalaturnyk (2005a,b, 2006) proposed a permeability model using an equivalent continuum approach based on geomechanics. Pan and Connell (2007) developed a theoretical model for sorption-induced strain and applied to single-component adsorption/strain experimental data. Clarkson (2008) recently expanded this theoretical model to calculate the sorption–strain component of the P&M model.

Robertson and Christiansen (2008) derived a coal permeability model for a fractured, sorptive-elastic medium, such as coal, under variable stress conditions. This model was derived for cubic geometry rather than matchstick geometry under biaxial or hydrostatic confining pressures. It was also designed to handle changes in permeability caused by adsorption and desorption of gasses from the matrix blocks. Contrary to previous models developed for field conditions, their model mainly deals with variable stress conditions which are commonly used during measurement of permeability in the laboratory. Similarly, Connell et al. (2010) presented two new analytical permeability models representing for standard triaxial strain and stress conditions. They presented a novel approach to distinguish the sorption strains of the coal matrix, the pores (or cleats) and the bulk coal. Based on the theory of poroelasticity, Zhang et al. (2008) developed a general porosity and permeability model. It was shown that current commonly used permeability models could be treated as specific examples.

When laboratory experimental results are interpreted, a matchstick or cubic coal model is typically assumed with the matrix blocks completely separated from each other in a stacked structure. In such a model, the permeability should not change under conditions of constant confining (total) stress due to through-going fracutres (Liu et al., 2011; Liu and Rutqvist, 2010). This interpretation is not consistent with laboratory observations (Harpalani and Chen, 1997; Pan et al., 2010; Pini et al., 2009), which show dramatic reduction in permeability with the injection of an adsorbing gas. Liu and Rutqvist (2010) assumed that coal matrix blocks connected each other by the coal-matrix bridges and developed a new coal-permeability model to explicitly consider fracture–matrix interaction during coal-deformation processes based on the concept of internal swelling stress. An alternate reasoning has been applied by Liu et al. (2010a, 2011) on this issue. They regarded that the above phenomena may be due to the ignorgance of the internal actions between coal fractures and matrix. Izadi et al. (2011) proposed a mechanistic representation of coal as a collection of unconnected cracks in an elastic swelling medium. The cracks are isolated from each other but swelling within a homogeneous but cracked continuum results in a reduction in crack aperture with swelling, and a concomitant reduction in permeability. Ma et al. (2011) developed a model based on the volumetric balance between the bulk coal, and solid grains and pores, and using the constant volume theory (Massarotto et al., 2009). It incorporates primarily the changes in grain and cleat volumes and is, therefore, different from the other models that lay heavy emphasis on the pore volume/cleat compressibility.

As reviewed above, a large variety of coal permeability models have been proposed. These span conditions representing constant stress through variable stress conditions. All of these coal permeability models were derived based on the theory of poroelasticity or equivalent continuum approach. Current experimental studies have been focusing on the overall behaviors of coal samples and only a few of them focus on the impact of fractures (Siriwardane et al., 2009).

Gas transport in coal seams is commonly represented as a dual porosity system accommodating two serial transport mechanisms: diffusion through the coal matrix then laminar flow through the cleat system (Bai and Elsworth, 2000; Elsworth and Bai, 1992). The permeability is primarily determined by the cleat aperture (Wu et al., 2010a, b; Zhang et al., 2008). The change in cleat aperture is a function of effective stress through poroelasticity, but coal swelling and shrinkage under a confining stress may also change the cleat aperture (Izadi et al., 2011; Wu et al., 2010a, b). Thus, the net change in coal permeability is a function of both the poroelastic response and the coal swelling or shrinkage.

Over the past few years, a series of advanced modeling tools has been developed to quantify the complex coal–gas interactions (Chen et al., 2009, Chen et al., 2010a, 2010b; Connell, 2009; Connell and Detournay, 2009; Gu and Chalaturnyk, 2005a,b, 2006; Liu et al., 2010a,b; Wu et al., 2010a,b, 2011; Zhang et al., 2008). These works have provided a coupling approach to represent important non-linear responses of coal matrix to the effective stress effects. *In this study, we used our poroelastic models to uncover the true reason why coal permeability switches from reduction to enhancement.* This goal was achieved through explicit

simulations of the dynamic interactions between coal matrix swelling/shrinkage and fracture aperture alteration, and translations of these interactions to perrmeability evolution under unconstrained boundary conditions.

2. General permeability model

It is clear that there is a relationship between porosity, permeability and the grain-size distribution in porous media. Chilingar (1964) defined this relationship as

$$k = \frac{d_e^2 \phi^3}{72(1-\phi)^2} \tag{1}$$

where k is the permeability, ϕ is porosity and d_e is the effective diameter of grains.

Based on this equation, one obtains

$$\frac{k}{k_0} = \left(\frac{\phi}{\phi_0}\right)^3 \left(\frac{1-\phi_0}{1-\phi}\right)^2. \tag{2}$$

When the porosity is much smaller than 1.0 (normally less than 10%), the second factor of the right-hand side asymptotes to unity. This yields the cubic relationship between permeability and porosity for the coal matrix

$$\frac{k}{k_0} = \left(\frac{\phi}{\phi_0}\right)^3 \tag{3}$$

Further, the coal porosity ratio evolves with the effective strain increment as

$$\frac{\phi}{\phi_0} = 1 + \frac{\alpha}{\phi_0}\Delta\varepsilon_e. \tag{4}$$

Therefore, the permeability ratio is evolved by

$$\frac{k}{k_0} = \left[1 + \frac{\alpha}{\phi_0}\Delta\varepsilon_e\right]^3 \tag{5}$$

where the effective strain increment is calculated by

$$\Delta\varepsilon_e = \Delta\varepsilon_v + \frac{\Delta p}{K_s} - \Delta\varepsilon_s \tag{6a}$$

or

$$\Delta\varepsilon_e = -\frac{\Delta\sigma - \Delta p}{K} \tag{6b}$$

where $\Delta\varepsilon_e$ is defined as the total effective volumetric strain, $\Delta\varepsilon_v$ is total volumetric strain increment, $\Delta p/K_s$ is coal compressive strain change, $\Delta\varepsilon_s$ is gas sorption-induced volumetric strain increment, and K_s represents the bulk modulus of coal grains.

Eqs. (4) and (5) are the formula for coal porosity and permeability. They are derived based on the fundamental principles of poroelasticity and can be applied to the evolution of coal porosity and permeability under variable boundary conditions. As shown in Eqs. (4) and (5), coal porosity and permeability can be expressed as a function of either effective strain (see Eq. (6a)) or effective stress (see Eq. (6b)).

3. Conceptual model

Coal is a typical dual porosity/permeability system (Warren and Root, 1963) containing porous matrix surrounded by fractures. These natural fractures form a closely-spaced network called cleats. The main set of fractures, termed face cleats, is comprised of well-developed, extensive, roughly planar fractures that run parallel to one another. Butt cleats are orthogonal to face cleats and often terminate at the face cleats. Butt cleats are also roughly planar but not as well-developed or as continuous as face cleats. The cleat system provides an essential and effective flow path for gas. Much of the measured bulk or "seam" permeability is due to the cleat system, although the presence of larger scale discontinuities such as fractures, joints, and faults can also make a significant contribution. The coal matrix is isolated by the fracture network and is the principal medium for storage of the gas, principally in adsorbed form and with low permeability in comparison to the bounding cleats (Gray, 1987). The surface area of the coal on which the methane is adsorbed is very large (20 to 200 m^2/g) (Patching, 1970) and gas is stored at near-liquid densities.The remaining gas is stored in the natural fractures, or cleats, either as free gas or dissolved in water.

In this study, we consider the interactions of the fractured coal mass where cleats do not create a full separation between adjacent matrix blocks but where solid rock bridges are present, as illustrated in Fig. 1. We accommodate the role of sorption-induced swelling strains both over contact bridges that hold cleat faces apart and over the non-contacting span between these bridges.

Fig. 1 illustrates the effective stress transfer between coal matrix and fracture induced by the CO_2 injection. Prior to the CO_2 injection, the gas pressure is equal in both fracture and matrix. This state is defined as the initial equilibrium state. The initial pore pressure is assumed to be zero, $p_m = p_f = 0$. Coal permeability at this state is defined as the initial equilibrium permeability. At this equilibrium state, no swelling takes place anywhere. We define this as the starting point for the evolution of permeability

$$\begin{cases} \dfrac{k}{k_0} = 1 \\ \sigma_{me} = \sigma_{fe} = 0 \cdot \end{cases} \tag{7}$$

When CO_2 is injected, the gas occupies the fracture and the gas pressure in the fracture reaches the injection pressure almost instantly. At this stage, the maximum inbalance beween fracture pressure and matrix pressure is achieved. This pressure inbalance is defined as

$$\begin{cases} \sigma_{me} = 0 \\ \sigma_{fe} = -\alpha p_f \end{cases}. \tag{8}$$

This inbalance diminishes as the gas diffuses into the coal matrix. The pore pressure in the matrix increases and in turn reduces the effective stress in matrix. As an outcome of the diffusion, coal matrix swells due to both the matrix pore pressure increase and the gas sorption. Initially, this matrix swelling is confined in the vicinity of the fracture voids. This localized swelling reduces the fracture aperture. This reduction in aperture reduces the fracture permeability. As the gas diffusion progresses, the swelling zone extends further into the coal matrix. As the swelling zone front moves away from the fracture void, the influence of matrix swelling on the fracture aperture weekens. As a result of the widening of the swelling zone, the fracture permeability recovers while the local swelling has become the macro-swelling. When the inbalace between fracture pressure and matrix pressure vanishes completely, the final equilibrium state is achieved. At the final equilibrium state, the matrix pressure is equal to the fracture pressure, i.e., $p_m = p_f$ which was defined as the ending point for the evolution of coal permeability.

$$\begin{cases} \sigma_{me} = -\alpha p_f \\ \sigma_{fe} = -\alpha p_f \end{cases} \tag{9}$$

Coal permeability at this state is defined as the final equilibrium permeability in which a uniform matrix swelling is achieved for a homogeneous coal sample.

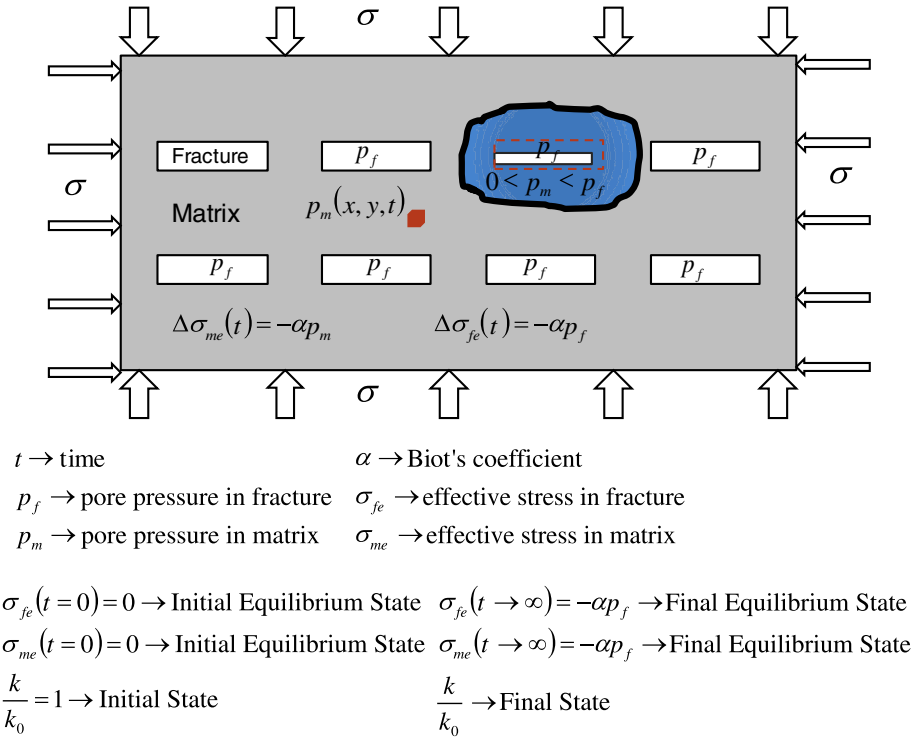

Fig. 1. Illustration of effective stress transfer between matrix and fracture and its impact on the evolution of coal permeability.

Fig. 2 illustrates the difference between local swelling and macro swelling. When the coal matrix swelling is localized in the vicinity of a fracture compartment, the effect of swelling acts competitively over these two components: increasing porosity and permeability due to swelling of the bridging contacts but reducing porosity and permeability due to the swelling of the intervening free-faces. When the coal matrix swelling is de-localized from the vicinity of a fracture compartment to the external boundary, the coal bridge swelling increases the fracture aperture while the coal matrix swelling changes the spacing only. At the uniform swelling state, as shown in Eq. (5), the coal permeability is determined by the coal bridge swelling only

$$\frac{k}{k_0}(t=\infty) = \left(1 + \varepsilon_L \frac{p_f}{p_L + p_f} - \frac{p_f}{K_s}\right)^3 \approx \left(1 + \varepsilon_L \frac{p_f}{p_L + p_f}\right)^3 \qquad (10)$$

where ε_L is the Langmuir strain constant, p_L is the Langmuir pressure, k is the coal permeability, and K_s is the coal grain bulk modulus. As shown in Eq. (10), coal permeability at the uniform matrix swelling state is not related to any elastic properties of coal at all.

Based on the above analysis, the final equilibrium permeability is always higher than the initial equilibrium permeability if a uniform swelling state is achieved within coal sample. However, laboratory measurements indicate that the coal equilibrium permeability is much lower than the initial equilibrium permeability at lower pore pressures. It may recover but rarely exceeds the initial equilibrium permeability even at higher pore pressures. This distinct discrepancy points that a uniform matrix swelling state has rarely been achieved in real coal samples. This implies that the transient characteristics of coal permeability are likely controlled by the localized swelling near the vicinity of coal fracture voids rather than the outside boundaries.

The pressure transient method (Brace et al., 1968; Hsieh et al., 1981) is normally used to conduct gas flow experiments in low permeability coal samples. In a typical experiment, the sample is placed into a triaxial core holder and both confining stress and axial stresses are applied at a rate of loading to establish initial conditions and are then kept constant. The sample-reservoir system is then vacuum desaturated to evacuate air from the system. A pressure increment is then applied to the upstream gas reservoir and discharged through the sample to the downstream gas reservoir. The time taken for the discharging upstream reservoir and the

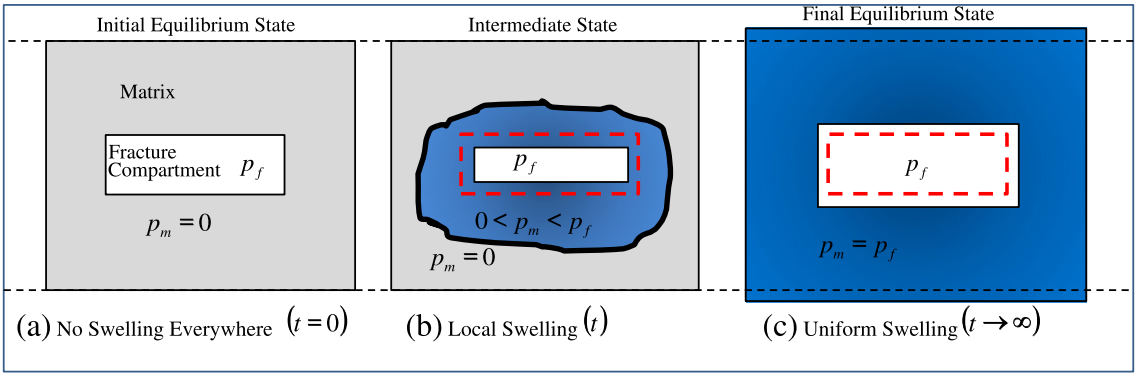

Fig. 2. Illustration of the difference between local swelling and macro swelling.

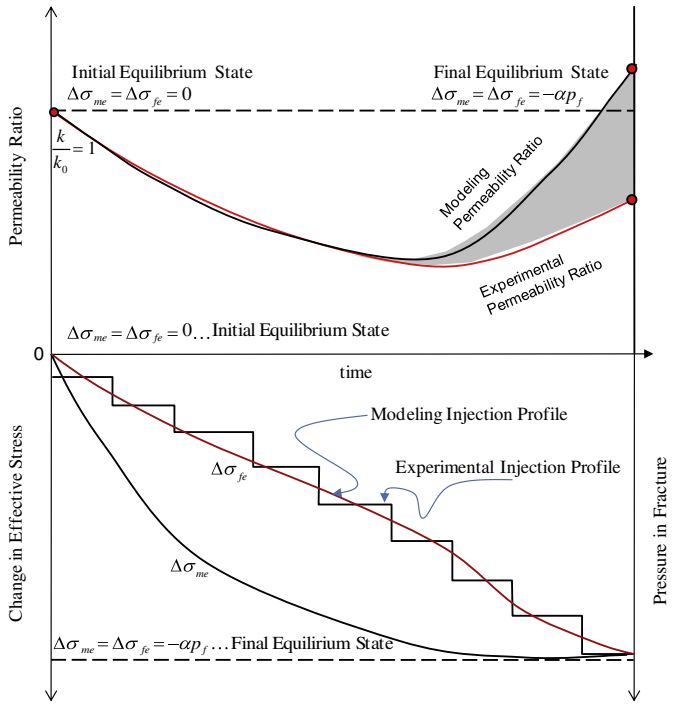

Fig. 3. Qualitative relations between complex processes triggered by CO_2 injection.

recharging downstream reservoir to reach a new equilibrium pressure is measured. This pattern is repeated for multiple cycles using the desired gas permeant. After multiple repeats of this procedure a relationship between permeability and pore pressure and effective stress is obtained. It is obvious that current laboratory measurements are only for the permeability at the final equilibrium state. For homogeneous coal samples, a net increase in permeability should be observed theoritically in the tests, as shown in Fig. 3.

Fig. 3. illustrates the evolution of coal permeability from the initial equilibrium state to the final equilibrium state and the associated effective stress transfer processes. The upper graph shows how the coal permeability ratio evolves from the initial state ($k/k_0 = 1$) to the final state ($k/k_0 = [1 + (\varepsilon_L p_f)/(p_L + p_f)]^3$). The ultimate permeability is calculated based on the assumption of a uniform swelling within the coal matrix. However, this condition may never be achieved for real coal samples. A difference of the ultimate permeability between an ideal homogeneous coal and a real heterogeneous coal is expected as shown in Fig. 3.

The lower part of Fig. 3 shows the evolution of effective stresses from the initial equilibrium, $\sigma_{fe} = \sigma_{me} = 0$, to the final equilibrium, $\sigma_{fe} = \sigma_{me} = -\alpha p_f$. For experiments, a step loading approach is normally used for the gas injection. In modeling, a smooth loading function can be used to approximate the step loading process. The step increments in fracture pressure or the smooth function approximation represent the effective stress change in the fracture. Correspondingly, the effective stress change in the matrix is represented by a smooth black line.

4. Quantitative model

In order to recover important non-linear responses due to effective stress effects, mechanical influence must be rigorously coupled with the gas transport system. This can be achieved through a full coupling approach. For this approach, a single set of equations (generally a large system of non-linear coupled partial differential equations) incorporating all of the relevant physics is solved simultaneously. Full coupling is often the preferred method for simulating multiple types of physics simultaneously since it should theoretically produce the most realistic results.

In the following section, a simulation model was constructed to investigate the permeability change under stress controlled conditions. The selected geometry is for a regular array of interacting cracks as shown in Fig. 4(b). The influence of effective stress and sorption-induced swelling response for an rectangular crack are examined. A single component part is removed from the array where the appropriate boundary conditions are for uniform displacement along the boundaries. This represents the symmetry of the displacement boundary condition mid-way between flaws as shown in Fig. 4(a). The simulation model geometry is 1.0 cm by 1.0 cm with a fracture located at the center. The fracure is 5 mm in length and 0.5 mm in width. Roller boundary was applied on the left side and bottom side, and the other two sides are stress control. No flow boundary was applied on all the outer boundaries and constant injection pressure was used along the fracrture boundaries. The change in aperture due to the combined influence of soprtion-induced swelling and effective stress was examined.

Input parameters for simulations were listed in Table 1. For the gas transport model, a time-dependent injection pressure was specified at the boundaries of fracture:

$$P_{in}(t) = \begin{cases} P_{init} + P_c\left(1 - e^{-\frac{t - t_p}{t_d}}\right) & t \geq t_p \\ P_{init} & t < t_p \end{cases} \quad (11)$$

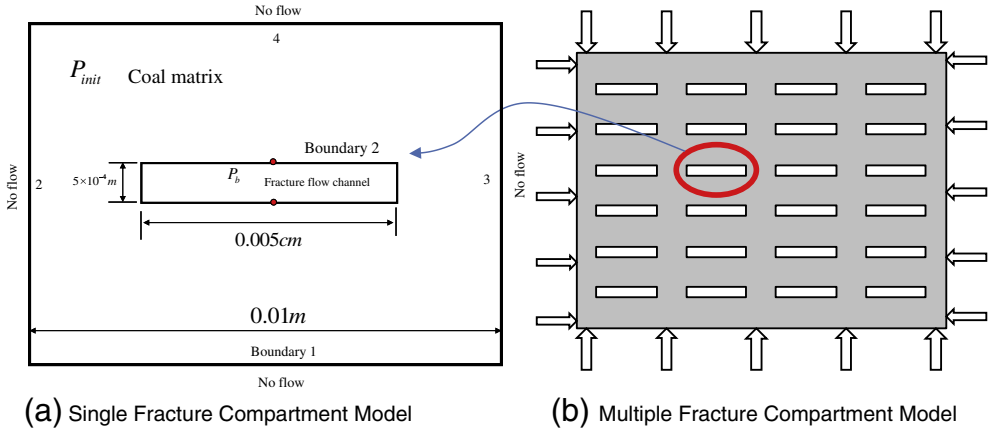

Fig. 4. Numerical model of a single fracture compartment to represent the response of multiple fracture compartment system under the unconstrained swelling condition. For deformation boundary: 1 and 2 are roller boundary; 3 and 4 are uniform tractions.

Table 1
Basic parameters in computations.

Parameter	Value
Porosity (%)	5.0
Matrix permeability (m^2)	10^{-20} or 10^{-23}
Gas viscosity (Pa s)	1.2278×10^{-5}
Young's modulus (GPa)	3.95
Poisson ratio	0.1
Biot's coefficient	0.66
Coal density (kg/m^3)	1500
Langmuir swelling strain	0.03
Langmuir sorption constant (m^3/kg)	0.01316
Langmuir pressure P_L (MPa)	3.96
Confining pressure (MPa)	12
Temperature (°C)	25
Universal gas constant ($m^3*Pa/(mol*K)$)	8.3144
Initial reservoir pressure (MPa)	0.1

where P_{init} is the initial reservoir pressure, and P_c is the pressure increment due to injection. The time t_d is the characteristic time to control loading speed. When the time t is less than t_p, no additional loading is applied. In computation, $t_p = 5s$.

The loading speed is

$$\frac{dP_{in}(t)}{dt} = \frac{P_c}{t_d} e^{-\frac{t-t_p}{t_d}}. \quad (12)$$

It is difficult to keep the constant $\frac{dP_{in}(t)}{dt}$ but we can keep the same

$$\frac{P_c}{t_d} = C. \quad (13)$$

If $P_c = 8MPa$ and $t_d = 1000s$, then $C = 8\times10^{-3}MPa/s$.

Table 2 shows the characteristic time for different equilibrium fracture pressures.

In this modeling example, the initial condition and the final condition are known. They are defined by Eqs. (7) and (10) except the initial reservoir pressure. Modeling results show how the coal permeability evolves from the initial state to the final state. For each case, the evolutions of coal permeability are plotted against pore pressure and time, respectively. Modeling behaviors are bounded by these two conditions. Comparisons between modeled equilibrium permeability and theoretical solution are shown in Fig. 5. This perfect match proves the validity of our modeling approach.

Modeling results for the case of $k = 10^{-20}m^2$ are shown in Fig. 6. In this example, five injection pressures from 2 MPa to 10 MPa were modeled with same loading rates. The temporal evolution of the coal permeablity is shown in Fig. 6(a). For all five cases, coal permeability experiences a rapid reduction at early stage, a switch in behavior from reduction to recovery, and a net increase at the final equilibrium state. The maximum reduction in permeability is proportional to the magnitude of the injection pressure. For example, the maximum reduction for $p_f = 2MPa$ is about 30% while the maximum reduction for $p_f = 10MPa$ is about 62%. The transitional period from reduction to recovery is inversely proportional to the magnitude of the injection pressure. For example, the transitional period for $p_f = 2MPa$ is about 1.0 h while the transitional period for $p_f = 10MPa$ is near instant. This

Table 2
Fracture pressure and characteristic time.

$P_c(MPa)$	2	4	6	8	10
$t_d(s)$	250	500	750	1000	1250

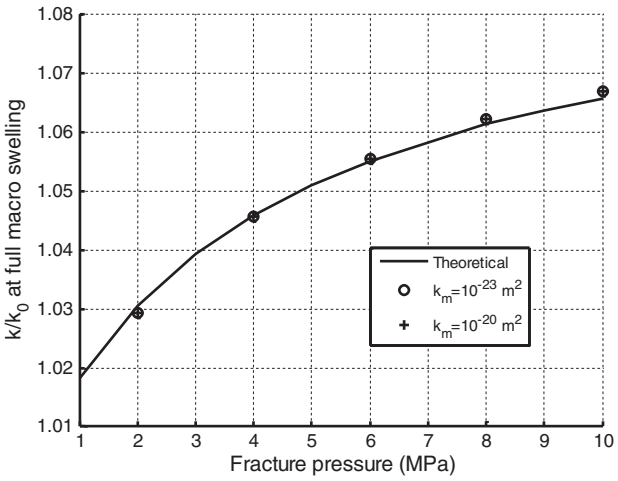

Fig. 5. Relation between final equilibrium permeability and fracture pressure.

numerical observation is important to the CO_2 injection, where the injection pressure is normally very high. Therefore, there could exist a sudden switch in behavior from permeability reduction to

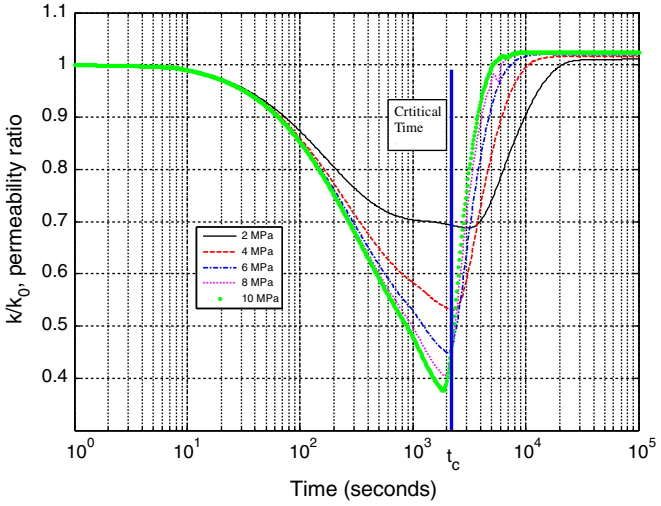

(a) Tempeoral evolution of coal permeability ratio

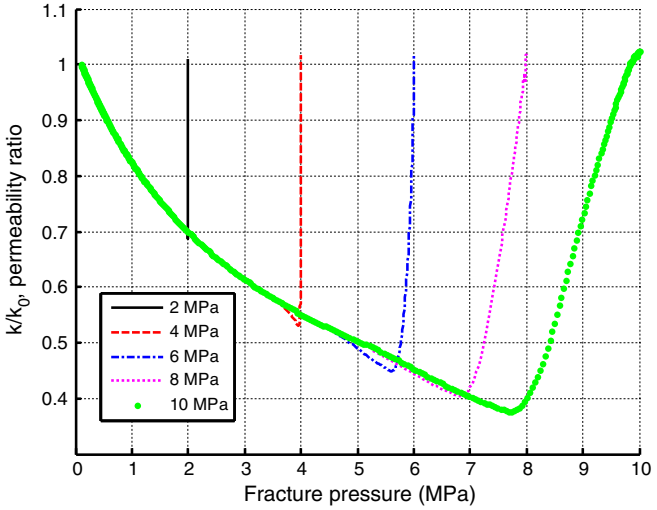

(b) Coal permeability ratio with pore pressure

Fig. 6. Evolutions of coal permeability for the case of $k = 10^{-20}m^2$.

permeability recovery and the transitional period is shorter for higher injection pressure .

The evolution of coal permeablity against the injection pressure is shown in Fig. 6(b). Prior to the CO_2 injection, the gas pressure in the fracture is equal to that in the matrix, $p_m = p_f = P_{init}$, the intial reservoir pressure. When CO_2 is injected, the gas occupies the fracture and the gas pressure in the fracture reaches the injection pressure almost instantly, i.e., $p_f = p_{in}$, where p_{in} is the injection pressure. At this stage, there exists an inbalance beween fracture pressure and matrix pressure. As a result of this inbalance, gas diffuses into the surrounding matrix block. In this process, the fracture supplies gas mass to the matrix block and the matrix pressure always lags the fracture pressure. At the initial stage, gas diffuses only into the vicinity of the fracture viod and local swelling controls the coal behavior. Because of the local swelling, coal permeability experiences rapid reduction for each loading step from 2*MPa* to 10*MPa*. This swelling-genearated permeability reduction is controlled by the internal (fracture) boundary. When local swelling becomes macro swelling, coal permeability recovers and this recovery is controlled by the external boundary condition. For all loading steps, the period of permeability reduction is much shorter than that of permeability recovery. As shown in Fig. 6(a), the period of permeability reduction is from 1000 *s* to 3000 *s* while that of permeability recovery from 10,000 *s* to 40,000 *s*. As shown in Fig. 6 (b), sharp switches in behavior are observed for lower loading step pressures from 2 *MPa* to 6 *MPa* while smooth switches in behavior are observed for higher step pressures from 8 *MPa* to 10 *MPa*. All of these observed behaviors are due to the fact that the matrix pressure always lags the fracture pressure.

Based on the above analysis, the permeability switch from reduction to recovery is corresponding to the matrix swelling switch from local swelling, controlled by the internal fracture boundaries, to macro swelling, controlled by the external boundaries. The switch behaviors of coal permeability and the matrix swelling are controlled by the same set of parameters including the initial coal permeability and the fracture spacing. For the same spacing, the switching behavior is primarily controlled by intial coal permeability. This is confirmed by our model results for the case of $k_0 = 10^{-23} m^2$, as shown in Fig. 7. In comparison with Fig. 6 for the case of $k_0 = 10^{-20} m^2$, the time to reach the final equilibrium state is much longer: $10^7 s$ for $k_0 = 10^{-23} m^2$ while $10^4 s$ for $k_0 = 10^{-20} m^2$. The magnitudes of coal initial permeability also affect permeability profiles: long stagnate periods are observed for the case of lower permeability before the local welling is switched to the macro swelling.

5. Development and evaluation of permeability switching model

5.1. Model development

Based on the above numerical analysis, a critical time is defined as t_c at which coal permeability switches from reduction to recovery. The pressure corresponding to this critical time, $p_c(t_c)$ or p_c, is defined as the critical pressure. Before the critical time, the matrix swelling is localized within the vicinity of the fracture void and the coal permeability is controlled by the internal fracture boundaries. The critical pressure is controlled by the coal properties such as initial permeability, fracture spacing, and injection process. When $p(t) \le p_c(t_c)$, coal swelling is confined within the vicinity of fractute compartments. The coal permeability is controlled by the local swelling. When local swelling controls, the coal permeability is determined by the internal volumetric transformations between matrix swelling and fracture void compaction. When $p(t) > p_c(t_c)$, coal swelling moves away from the vicinity of fractute compartments to external boundaires. The coal permeability is controlled by macro swelling. When the macro swelling controls, the coal permeability is determined by the balance between total volume change and internal volume transformation. These distinct behaviors are approximated as follows: the total strain is assumed as zero, $\Delta\varepsilon_v = 0$, when local swelling controls; $\Delta\varepsilon_v \neq 0$ when macro swelling controls. Under this approximation, Eq. (5) can be extended into

$$\frac{k}{k_0} = \begin{cases} \left[1 + \frac{\alpha}{\varphi_0}\left(-\Delta\varepsilon_s + \frac{p}{K_s}\right)\right]^3 & p \le p_c \\ \left[1 + \frac{\alpha}{\varphi_0}\left(-\frac{\varepsilon_L p_c}{p_c + p_L} + \frac{p_c}{K_s}\right)\right]^3 \left[1 + \frac{\alpha}{\varphi_0}\left(\Delta\varepsilon_v - \frac{\varepsilon_L (p - p_c)}{p - p_c + p_L} + \frac{p - p_c}{K_s}\right)\right]^3 & p > p_c \end{cases} \quad (14)$$

For the stress controlled experiments, Eq. (14) is simplifed as

$$\frac{k}{k_0} = \begin{cases} \left[1 + \frac{\alpha}{\varphi_0}\left(-\Delta\varepsilon_s + \frac{p}{K_s}\right)\right]^3 & p \le p_c \\ \left[1 + \frac{\alpha}{\varphi_0}\left(-\frac{\varepsilon_L p_c}{p_c + p_L} + \frac{p_c}{K_s}\right)\right]^3 \left[1 + \frac{\alpha}{\varphi_0}\left(\frac{p - p_c}{K}\right)\right]^3 & p > p_c \end{cases} \quad (15)$$

5.2. Model verification

In order to verify Eq. (15), an experiment was performed on anthracite coal from the Northumberland Basin, Pennsylvania. Detailed description of the experiment can be found in Wang et al.

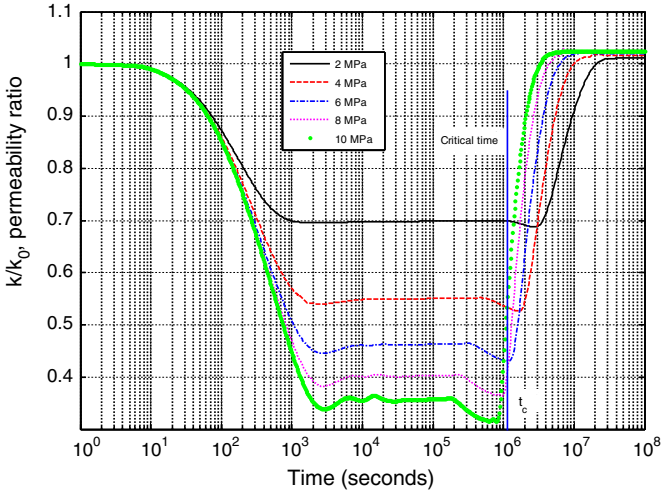

(a) Temporal evolution of coalpermeability ratio

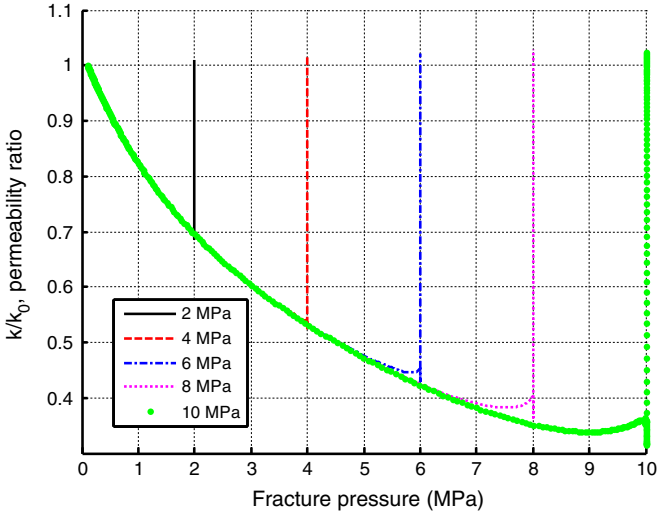

(b) Coal permeability ratio with pore pressure

Fig. 7. Evolutions of coal permeability for the case of $k = 10^{-23} m^2$.

(2011). The sample was drilled parallel to the bedding plane. A roughness of 3 on Barton's scale (Barton, 1976) is estimated for bedding planes in this coal. The cleat aperture is approximately 10–50 μm. The mean density of the coal under unconfined conditions was calculated from the mass and volume of the three cylindrical cores, and yielded an average matrix density of 1397.9 kg m^{-3}. In the laboratory tests, permeability evolution was measured with respect to pore pressure at constant total stresses of 12 *MPa*. At a total stress of 12 *MPa* the permeability to CO_2 first decreases by 86% (pore pressure of 1.15 to 2.22 *MPa*) and then rebounds to a net 19% reduction over the initial permeability at the final pore pressure of 4.58 *MPa*. In this match, the following papameters were assumed: $\varphi_f = 0.005$, $R_m = 0$, $\varepsilon_L = 0.015$, $K_s = 500MPa$, and $p_L = 6MPa$. The critical pressure is measured as $p_c = 2.5MPa$. As shown in Fig. 8, the match between the modeled curve and the measured data is quite good.

5.3. Model evaluation

There is a large variety of coal permeability models. These span conditions representing constant stress through variable stress conditions. A matchstick or cubic coal model is typically assumed with matrix blocks completely separated from each other in a coal sample. In this arrangement matrix swelling will not affect coal fracture permeability under the constant confining (total) stress conditions, because, for a given pore pressure, the coal matrix swelling will result in swelling of the blocks alone, rather than changes in fracture aperture. The ambient effective stress also exerts no influence on matrix swelling, due to the complete separation between matrix blocks caused by through-going fractures. Therefore, the permeability should not change. In other words, 0% of the swelling/shrinkage strain contributes to the coal permeability change. However, when the coal sample is completely constrained from all directions, the coal matrix swelling will be completely transferred to the reduction in fracture apertures. In this situation, 100% of the swelling/shrinkage strain contributes to the coal permeability change provided the fractures are much more compliant than the coal matrix. Relations between theoretical solutions for these two extreme cases and the critical pressure are defined as

$$\frac{k}{k_0} = \left[1 + \frac{\alpha}{\varphi_0}\left(\frac{p}{K}\right)\right]^3 \quad p_c = 0 \rightarrow \text{Unconstrained Swelling} \tag{16}$$

$$\frac{k}{k_0} = \left[1 - \frac{\alpha}{\varphi_0}\left(\frac{\varepsilon_L p}{p + p_L}\right)\right]^3 \quad p_c = \infty \rightarrow \text{Constrained Swelling.} \tag{17}$$

Eqs. (16) and (17) represent two extreme cases. Their solutions bound the true behavior of coal permeability. Example solutions are illustrated in Fig. 9. These illustrations are consistent with typical laboratory observations. Direct observations of the influence of coal swelling on permeability change were made by Robertson (2005). In his study, four different gasses (helium, N_2, CH_4 and CO_2) were injected into coal samples. Similar experiments have been conducted by others (Kiyama et al., 2011; Pini et al., 2009; Siriwardane et al., 2009; Wang et al., 2010). These observations demonstrate that even under controlled stress conditions the injection of adsorptive gasses reduces the coal permeability at a lower gas pressure and the coal permeability might rebound at a higher gas pressure. This observed switch in behavior is presumably due to the dependence of coal swelling on the gas pressure: coal swelling diminishes at high pressures. Further, the illustrations in Fig. 9 are also consistent with typical in-situ observations. In-situ measured data show that the absolute permeability of coal gas reservoirs increases significantly with continued gas production (Cherian et al., 2010; Clarkson, 2008; Sparks et al., 1995; Young et al., 1991). This phenomenon causes gas-production rate to be many times greater than expected. This phenomenon also caused bottom hole pressures to increase when gas rate was constant, opposite from that expected from conventional applications of Darcy's law. The opposite observation was made when CO_2 was injected to enhance CBM production. One example is the Allison Unit CO_2 enhanced coalbed methane recovery pilot project, located in the northern New Mexico portion of the San Juan Basin. Reeves et al. (2003) reported the evidence of significant coal permeability reduction with CO_2 injection. Another example is the CO_2-ECBM pilot project in Qinshui Basin, China. It has been reported that the CO_2 injectivity decreased during injection but permeability rebounded after an extended production period of one month (Wong et al., 2007). Similar observations were also made in other ECBM pilot projects (Koperna et al., 2009).

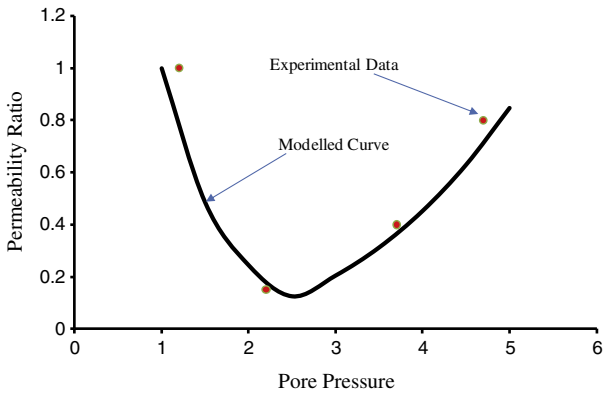

Fig. 8. Verfication of permeability switching model against experimental data.

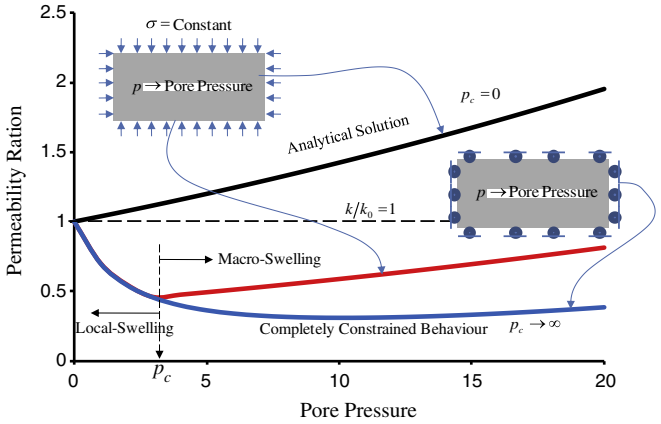

Fig. 9. Comparisons of permeability switching model results with analytical solutions of constrained swelling and unconstrained swelling.

6. Conclusions

A full coupling approach was applied to recover important non-linear responses due to the effective stress effects during the mechanically unconstrained (stress-controlled) swelling. Based on our model results, the following major conclusions were drawn:

- At the initial stage of CO_2 injection, matrix swelling is localized within the vicinity of the fracture compartment. As the injection continues, the swelling zone is widening further into the matrix and becomes macro-swelling. Matrix properties control the swelling transition from local swelling to macro swelling.
- Matrix swelling processes control the evolution of coal permeability. When the swelling is localized, coal permeability is controlled by the internal fracture boundary condition and behaves volumetrically; when the swelling becomes macro-swelling, coal permeability is

controlled by the external boundary condition and behaves non-volumetrically.

- Matrix properties control the switch in swelling behavior from local swelling to macro swelling and the associated switch in permeability behavior from reduction to recovery. A coal permeability model has been developed to represent this switching behavior in coal permeability under variable stress conditions. Model predictions are consistent with typical laboratory and in-situ observations available in the lietrature.

Acknowledgments

This work is a partial result of support from CSIRO Flagship top-up scholarship, NIOSH under contract 200-2008-25702, Major State Basic Research Development Program Fund (grant no. 2010CB226801) and the State Administration of Foreign Experts Affairs, PR China (TS2011ZGKY [BJ]019). These sources of support are gratefully acknowledged.

References

Bai, M., Elsworth, D., 2000. Coupled Processes in Subsurface Deformation, Flow and Transport. ASCE Press. 336 pp.
Barton, N., 1976. The shear strength of rock and rock joints. International Journal of Rock Mechanics and Mining Sciences & Geomechanics Abstracts 13, 255–279.
Brace, W.F., Walsh, J.B., Frangos, W.T., 1968. Permeability of granite under high pressure. Journal of Geophysical Research 73 (6), 2225–2236.
Chen, Z., Liu, J., Elsworth, D., Connell, L., Pan, Z., 2009. Investigation of CO_2 injection induced coal-gas interactions. 43rd U.S. Rock Mechanics Symposium & 4th U.S.-Canada Rock Mechanics Symposium. American Rock Mechanics Association, Asheville, North Carolina.
Chen, Z., Liu, J., Elsworth, D., Connell, L.D., Pan, Z., 2010a. Impact of CO_2 injection and differential deformation on CO_2 injectivity under in-situ stress conditions. International Journal of Coal Geology 81 (2), 97–108.
Chen, Z., Liu, J., Pan, Z., Connell, L., Elsworth, D., 2010b. Relations between coal permeability and directional strains and their application to San Juan Basin. 44th U.S. Rock Mechanics Symposium and 5th U.S.-Canada Rock Mechanics Symposium. American Rock Mechanics Association, Salt Lake City, Utah.
Chen, Z., Pan, Z., Liu, J., Connell, L.D., Elsworth, D., 2011. Effect of the effective stress coefficient and sorption-induced strain on the evolution of coal permeability: experimental observations. International Journal of Greenhouse Gas Control. doi:10.1016/j.ijggc.2011.07.005.
Cherian, B.V., Claugus, A., Dilli, M., Mata, D., Sitchler, J.C., Alatrach, S., Neumiller, J., Panjaitan, M., 2010. An Integrated single-well approach to evaluating completion effectiveness and reservoir properties in the Wind Dancer Field. Tight Gas Completions Conference, San Antonio, Texas, USA, SPE 137126.
Chilingar, G.V., 1964. Relationship between porosity, permeability, and grain-size distribution of sands and sandstones. In: Straaten, L.M.J.U.v. (Ed.), Developments in Sedimentology. Elsevier, pp. 71–75.
Clarkson, C.R., 2008. Case study: production data and pressure transient analysis of horseshoe Canyon CBM wells. CIPC/SPE Gas Technology Symposium 2008 Joint Conference, Calgary, Alberta, Canada.
Connell, L.D., 2009. Coupled flow and geomechanical processes during gas production from coal seams. International Journal of Coal Geology 79 (1–2), 18–28.
Connell, L.D., Detournay, C., 2009. Coupled flow and geomechanical processes during enhanced coal seam methane recovery through CO_2 sequestration. International Journal of Coal Geology 77 (1–2), 222–233.
Connell, L.D., Lu, M., Pan, Z., 2010. An analytical coal permeability model for tri-axial strain and stress conditions. International Journal of Coal Geology 84 (2), 103–114.
Cui, X., Bustin, R.M., 2005. Volumetric strain associated with methane desorption and its impact on coalbed gas production from deep coal seams. AAPG Bulletin 89 (9), 1181–1202.
Durucan, S., Edwards, J.S., 1986. The effects of stress and fracturing on permeability of coal. Mining Science and Technology 3 (3), 205–216.
Elsworth, D., Bai, M., 1992. Flow-deformation response of dual porosity media. Journal of Geotechnical Engineering 118 (1), 107–124.
Gilman, A., Beckie, R., 2000. Flow of coal-bed methane to a gallery. Transport in Porous Media 41 (1), 1–16.
Gray, I., 1987. Reservoir engineering in coal seams: part 1—the physical process of gas storage and movement in coal seams. SPE Reservoir Engineering 2 (1), 28–34.
Gu, F., Chalaturnyk, J.J., 2005a. Analysis of coalbed methane production by reservoir and geomechanical coupling simulation. Journal of Canadian Petroleum Technology 44 (10), 33–42.
Gu, F., Chalaturnyk, R.J., 2005b. Sensitivity study of coalbed methane production with reservoir and geomechanic coupling simulation. Journal of Canadian Petroleum Technology 44 (10), 23–32.
Gu, F., Chalaturnyk, R.J., 2006. Numerical simulation of stress and strain due to gas sorption/ desorption and their effects on in-Situ permeability of coalbeds. Journal of Canadian Petroleum Technology 45 (10), 52–62.
Han, F., Busch, A., Wageningen, N., Yang, J., Liu, Z., Krooss, B.M., 2010. Experimental study of gas and water transport processes in the inter-cleat (matrix) system of coal: anthracite from Qinshui Basin, China. International Journal of Coal Geology 81 (2), 128–138.
Harpalani, S., Chen, G., 1997. Influence of gas production induced volumetric strain on permeability of coal. Geotechnical and Geological Engineering 15 (4), 303–325.
Harpalani, S., Schraufnagel, R.A., 1990. Shrinkage of coal matrix with release of gas and its impact on permeability of coal. Fuel 69 (5), 551–556.
Hsieh, P.A., Tracy, J.V., Neuzil, C.E., Bredehoeft, J.D., Silliman, S.E., 1981. A transient laboratory method for determining the hydraulic properties of 'tight' rocks–I. Theory. International Journal of Rock Mechanics and Mining Sciences & Geomechanics Abstracts 18 (3), 245–252.
Izadi, G., Wang, S., Elsworth, D., Liu, J., Wu, Y., Pone, D., 2011. Permeability evolution of fluid-infiltrated coal containing discrete fractures. International Journal of Coal Geology 85 (2), 202–211.
Kiyama, T., Nishimoto, S., Fujioka, M., Xue, Z., Ishijima, Y., Pan, Z., Connel, L.D., 2011. Coal swelling strain and permeability change with injecting liquid /supercritical CO_2 and N_2 at stress-constrained conditions. International Journal of Coal Geology 85 (1), 56–64.
Koperna, G.J., Oudinot, A.Y., McColpin, G.R., Liu, N., Heath, J.E., Wells, A., Young, G.B., 2009. CO_2-ECBM /storage activities at the San Juan Basin's pump Canyon test site. SPE Annual Technical Conference and Exhibition, New Orleans, Louisiana, SPE 124002.
Liu, H.-H., Rutqvist, J., 2010. A new coal permeability model: internal swelling stress and fracture–matrix interaction. Transport in Porous Media 82 (1), 157–171.
Liu, J., Chen, Z., Elsworth, D., Miao, X., Mao, X., 2010a. Linking gas-sorption induced changes in coal permeability to directional strains through a modulus reduction ratio. International Journal of Coal Geology 83 (1), 21–30.
Liu, J., Chen, Z., Elsworth, D., Miao, X., Mao, X., 2010b. Evaluation of stress-controlled coal swelling processes. International Journal of Coal Geology 83 (4), 446–455.
Liu, J., Chen, Z., Elsworth, D., Qu, H., Chen, D., 2011. Interactions of multiple processes during CBM extraction: a critical review. International Journal of Coal Geology. doi:10.1016/j.coal. 2011.06.004.
Ma, Q., Harpalani, S., Liu, S., 2011. A simplified permeability model for coalbed methane reservoirs based on matchstick strain and constant volume theory. International Journal of Coal Geology 85 (1), 43–48.
Massarotto, P., Golding, S.D., Rudolph, V., 2009. Constant volume CBM reservoirs: an important principle. International Coalbed Methane Symposium, Tuscaloosa, Alabama.
Mazumder, S., Wolf, K.H., 2008. Differential swelling and permeability change of coal in response to CO_2 injection for ECBM. International Journal of Coal Geology 74 (2), 123–138.
Palmer, I., Mansoori, J., 1996. How permeability depends on stress and pore pressure in coalbeds: a new model. 1996 Copyright 1996 SPE Annual Technical Conference and Exhibition. Society of Petroleum Engineers, Inc., Denver, Colorado.
Palmer, I.D., Mavor, M., Gunter, B., 2007. Permeability changes in coal seams during production and injection. International Coalbed Methane Symposium, University of Alabama, Tuscaloosa, Alabama. Paper 0713.
Pan, Z., Connell, L.D., 2007. A theoretical model for gas adsorption-induced coal swelling. International Journal of Coal Geology 69 (4), 243–252.
Pan, Z., Connell, L.D., Camilleri, M., 2010. Laboratory characterisation of coal reservoir permeability for primary and enhanced coalbed methane recovery. International Journal of Coal Geology 82 (3–4), 252–261.
Patching, T.H., 1970. Retention and release of gas in coal—a review. Canadian Mining and Metallurgical Bulletin 63 (703), 1302–1308.
Pekot, L.J., Reeves, S.R., 2002. Modeling the effects of matrix shrinkage and differential swelling on coalbed methane recovery and carbon sequestration. U.S. Department of Energy DE-FC26-00NT40924.
Pini, R., Ottiger, S., Burlini, L., Storti, G., Mazzotti, M., 2009. Role of adsorption and swelling on the dynamics of gas injection in coal. Journal of Geophysical Research 114 (B4), B04203.
Reeves, S., Taillefert, A., Pekot, L., Clarkson, C., 2003. The Allison unit CO_2-ECBM pilot: a reservoir modelling study. Topical Report, U.S. Department of Energy, DE-FC26-0NT40924. (February).
Reiss, L.H., 1980. The Reservoir Engineering Aspects of Fractured Formations. Gulf Publishing Co., Houston.
Robertson, E.P., 2005. Modeling permeability in coal using sorption-induced strain data. SPE Annual Technical Conference and Exhibition. Society of Petroleum Engineers, Dallas, Texas.
Robertson, E.P., Christiansen, R.L., 2008. A permeability model for coal and other fractured, sorptive-elastic media. SPE Journal 13 (3), 314–424.
Seidle, J.R., Huitt, L.G., 1995. Experimental measurement of coal matrix shrinkage due to gas desorption and implications for cleat permeability increases. 1995 Copyright 1995 International Meeting on Petroleum Engineering. Society of Petroleum Engineers, Inc., Beijing, China.
Shi, J.-Q., Durucan, S., 2004a. A numerical simulation study of the Allison unit CO_2 -ECBM pilot: the impact of matrix shrinkage and swelling on ECBM production and CO_2 injectivity. Proceedings of 7th International Conference on Greenhouse Gas Control Technologies.
Shi, J.Q., Durucan, S., 2004b. Drawdown induced changes in permeability of coalbeds: a new interpretation of the reservoir response to primary recovery. Transport in Porous Media 56 (1), 1–16.
Siriwardane, H., Haljasmaa, I., McLendon, R., Irdi, G., Soong, Y., Bromhal, G., 2009. Influence of carbon dioxide on coal permeability determined by pressure transient methods. International Journal of Coal Geology 77 (1–2), 109–118.
Somerton, W.H., Söylemezoglu, I.M., Dudley, R.C., 1975. Effect of stress on permeability of coal. International Journal of Rock Mechanics and Mining Sciences & Geomechanics Abstracts 12 (5–6), 129–145.
Sparks, D.P., McLendon, T.H., Saulsberry, J.L., Lambert, S.W., 1995. The effects of stress on coalbed reservoir performance, Black Warrior Basin. U.S.A. SPE Annual Technical Conference and Exhibition, Dallas, Texas.

Wang, G.X., Wei, X.R., Wang, K., Massarotto, P., Rudolph, V., 2010. Sorption-induced swelling/ shrinkage and permeability of coal under stressed adsorption/desorption conditions. International Journal of Coal Geology 83 (1), 46–54.

Wang, S., Elsworth, D., Liu, J., 2011. Permeability evolution in fractured coal: the roles of fracture geometry and water-content. International Journal of Coal Geology 87, 13–25.

Warren, J.E., Root, P.J., 1963. The behavior of naturally fractured reservoirs. Society of Petroleum Engineers Journal 3 (3), 245–255.

Wong, S., Law, D., Deng, X., Robinson, J., Kadatz, B., Gunter, W.D., 2007. Enhanced coalbed methane and CO_2 storage in anthracitic coals—Micro-pilot test at South Qinshui, Shanxi, China. International Journal of Greenhouse Gas Control 1 (2), 215–222.

Wu, Y., Liu, J., Elsworth, D., Chen, Z., Connel, L., pan, Z., 2010a. Dual poroelastic response of a coal seam to CO_2 injection. International Journal of Greenhouse Gas Control 4 (4), 668–678.

Wu, Y., Liu, J., Elsworth, D., Miao, X., Mao, X., 2010b. Development of anisotropic permeability during coalbed methane production. Journal of Natural Gas Science and Engineering 2 (4), 197–210.

Wu, Y., Liu, J., Chen, Z., Elsworth, D., Pone, D., 2011. A dual poroelastic model for CO_2-enhanced coalbed methane recovery. International Journal of Coal Geology 86 (2–3), 177–189.

Young, G.B.C., McElhiney, J.E., Paul, G.W., McBane, R.A., 1991. An analysis of Fruitland coalbed methane production, Cedar Hill Field, Northern San Juan Basin. SPE Annual Technical Conference and Exhibition, Dallas, Texas.

Zhang, H., Liu, J., Elsworth, D., 2008. How sorption-induced matrix deformation affects gas flow in coal seams: a new FE model. International Journal of Rock Mechanics and Mining Sciences 45 (8), 1226–1236.